Spectrally encoded photoacoustic microscopy using a digital mirror device

Yu Wang
Konstantin Maslov
Lihong V. Wang

Spectrally encoded photoacoustic microscopy using a digital mirror device

Yu Wang, Konstantin Maslov, and Lihong V. Wang
Washington University in St. Louis, Optical Imaging Laboratory, Department of Biomedical Engineering, 1 Brookings Drive, St. Louis, Missouri 63130

Abstract. We have developed spectrally encoded photoacoustic microscopy using a digital mirror device for multi-wavelength tomography, which enables fast spectral imaging of optical absorption. The optical illumination wavelengths are multiplexed at a laser pulse repetition rate of ~2 kHz. Liquid samples, whole blood, and blood vessels in mouse ears were imaged. Compared with internal wavelength tuning of a narrow-band laser, external wavelength tuning based on a digital mirror device improves the data acquisition speed of spectral photoacoustic microscopy. Compared with external wavelength scanning of a wide-band laser with the same pulse energy, spectral encoding improves the signal-to-noise ratio. © 2012 Society of Photo-Optical Instrumentation Engineers (SPIE). [DOI: 10.1117/1.JBO.17.6.066020]

1 Introduction

Spectral (i.e., multi-wavelength) photoacoustic (PA) tomography provides *in vivo* label-free optical absorption measurements, enabling structural, functional, and molecular imaging of either fluorescent or nonfluorescent tissue chromphores.[1,2] It is based on the detection of ultrasonic waves generated by tissue chromophores that have absorbed pulsed or modulated light. This technique commonly used tunable excitation laser systems, such as a dye laser,[3] a Ti:sapphire laser,[4] or an optical parametric oscillator laser.[5] These laser sources provide laser pulses with nanojoule to millijoule pulse energy and nanosecond duration in the visible and near-infrared range, yet they suffer inherent difficulty in tuning the excitation wavelength quickly enough for measuring optical absorption spectra in dynamic processes *in vivo*. Fast wavelength tuning reduces the time to acquire a stack of multi-wavelength PA images so that dynamic processes such as oxygen release from moving red blood cells can be spectrally quantified. Moreover, for *in vivo* imaging, it mitigates the motion artifact so that multi-wavelength images can be precisely co-registered.

A straightforward approach to speed up multi-wavelength PA imaging is to use a broadband pulsed light source with an external tunable optical filter, which transmits a selected wavelength of light at a time.[6,7] By rapidly scanning across the individual wavelengths, optical absorption spectra are measured. However, optical filtering by excluding all wavelengths but one from the broadband laser beam is not energy-efficient. Although the PA signal-to-noise ratio (SNR) for tunable-laser-based PA microscopy is usually limited by the ANSI safety standard,[8] broadband sources, such as a photonic crystal fiber laser[7] or a laser diode array,[9] have such low pulse spectral densities that their pulse energy levels become the limiting factor for the PA SNR. For example, Takashi et al. built a wavelength-agile PA microscope using a photonic crystal fiber supercontinuum source.[7] Because of the inadequacy in pulse energy and spectral density, the bandwidth of the tunable band pass filter had to be widened to 40 nm around each tuned wavelength, which significantly sacrificed spectral resolution and made separation of different optical absorbers challenging.

Here we present a spectral encoding approach that exploits a wide illumination spectrum by using a digital mirror device (DMD) as a wavelength selecting element. The DMD can multiplex light of a large number of arbitrary illumination wavelengths at a pulse repetition rate of up to 22 kHz. Thus the spectrally encoded PA imaging system can deliver multiple wavelengths simultaneously, significantly increasing the PA SNR.

Figure 1(a) shows a schematic of the optical layout of the spectrally encoded PA microscopy system, which used a Nd: YLF laser (INNOSLAB, Edgewave) pumped circulating laser dye cell (PC-1000, Sirah) as the broadband light source. To extend the lasing spectral range, the circulating dye cell contained a binary mixture of 25 mg/L Rhodamine 6G and 3 mg/L Rhodamine B ethanol solution.[10] The emerging broadband laser beam had a full width at half maximum emission spectral range of 574 to 586 nm [Fig. 1(b)]. The light was spatially filtered by a 50 μm diameter pinhole and collimated on to a transmission diffraction grating (600 lines/mm blazed at 560 nm, Wasatch Photonics). The spectrally dispersed output of the diffraction grating was imaged by a cylindrical lens with a focal length of 300 mm on to the surface of the DMD (Discovery 4100, Texas Instruments) with a linear dispersion of 5.5 nm/mm. The cylindrical lens was oriented to focus to a vertical line, so that each of the DMD columns corresponded to a different wavelength within the illumination spectral range.[11] The DMD had 1024 columns and 768 rows of microscopic mirrors with a pitch size of 13.68 μm, which could be individually tilted clockwise or counterclockwise ($\pm$12 deg) from the DMD normal, to an "on" or "off" state. Because
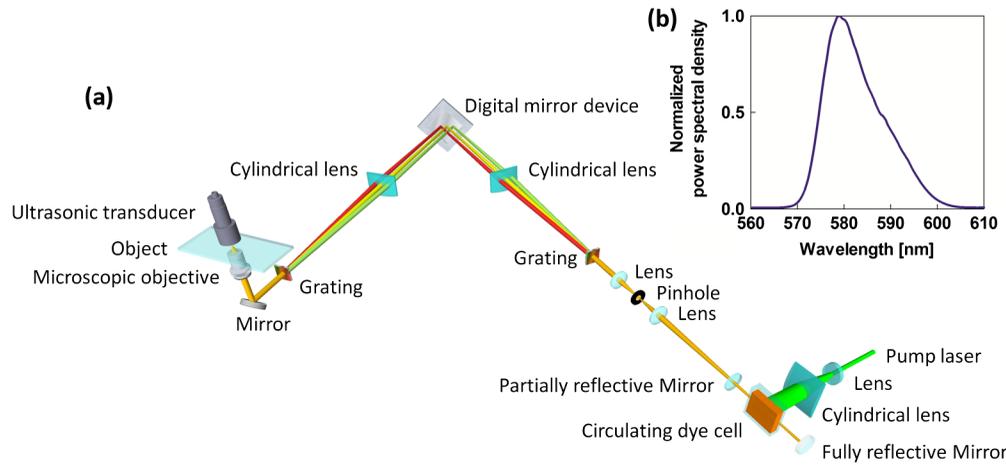
Fig. 1 (a) Schematic of the spectrally encoded PA microscopy system. (b) Emission spectrum of the broadband source, i.e., the output from the circulating dye cell.

the mirror elements rotate on their diagonal axes, the DMD was mounted at 45 deg so that the diagonal axes are vertical to keep the reflected illumination beams in the horizontal plane. By changing the angular pattern of the DMD, the "on" state mirrors selected the wavelengths from the broadband optical illumination spectrum. The laser light at the selected wavelengths was collimated by a cylindrical lens on to another diffraction grating, oriented so that spectrally dispersed light was recombined spatially. The spectrally encoded illumination was then delivered to a PA microscopy module,[12] consisting of a microscopic objective and an ultrasonic transducer that were coaxially and confocally aligned. The laser pulse generation, DMD control, and data acquisition were synchronized through the TTL signal pulses generated by the motion controller at 1.91 kHz. The imaging speed was limited by the laser pulse repetition rate. Optical absorption spectra were collected photoacoustically with 15 bins over a spectral range of 574 to 586 nm, yielding a spectral resolution of 0.9 nm. The biological tissue was mechanically scanned in the x-y plane to construct a three-dimensional image of the optical absorption distribution.

The DMD-based wavelength tuning mechanism based on pixelated modulation enables not only fast quantitative spectral imaging but also more energy-efficient manipulation of the illumination wavelengths. Wavelength multiplexing in Hadamard transform spectroscopy has proven effective in improving the signal-noise-ratio (SNR) of spectral measurements.[13,14] Compared with a single-wavelength slit, the encoding mask used in Hadamard spectroscopy increases light collection efficiency over an extended wavelength range, thus improving the SNR of spectral measurements. In our study, a wavelength multiplexing pattern defined by the Hadamard S-matrix was employed in the same way as in Hadamard transform spectroscopy.[13] A wavelength multiplexing pattern consisting of 15-element binary Hadamard S-sequence masks was used for a 15-bin spectrum. The S-sequence had eight entries that were ones and seven that were zeros. Instead of recording the PA signal for one wavelength at a time, eight wavelengths were selected at the same time. Instead of scanning through the 15 wavelengths one by one, 15 measurements with different combinations of eight wavelengths were made. The illumination wavelengths were configured between PA measurements in such a way that a complete 15-bin spectrum can be recovered as follows:

$$P_I = S_{15}^{-1} \cdot P_H, \qquad (1)$$

where P_I is the recovered PA amplitude vector at 15 individual spectral bins, P_H is the PA amplitude vector measured using 15 DMD-encoded S-sequence masks, S_{15} is the 15-order Hadamard S-matrix, and the superscript -1 denotes matrix inversion. With noise mainly limited by the ultrasonic transducer, this approach improved the PA amplitude SNR compared with the external wavelength scanning method.

To demonstrate the system's capability in fast spectral measurement, two liquid samples were imaged, including DODCI (06480, Exciton) ethyl alcohol solution of 1-M concentration and whole bovine blood (910, Quad Five). The samples were individually sealed in sample well plates using transparent polyethylene membrane. At 586 nm, the DODCI solution and whole bovine blood had absorption coefficients of 306 cm^{-1} and 148 cm^{-1}, respectively. Figure 2 compares the optical absorption spectra acquired by scanning the optical wavelength from 574 to 586 nm and by using spectrally encoded PA measurement. The laser pulse energy was first set to ~15 nJ at 586 nm, and the PA scanning measurement is referred to as "high-energy wavelength scanning." Because the focal diameter of the laser beam was 5 μm, the laser fluence was 76 mJ/cm^2. The absorption coefficients were quantified in relative units using the peak amplitude values of the Hilbert-transformed PA A-line signals.[15]

Compared with the gold-standard spectrophotometer measurements (Cary 50, Varian), the high-energy wavelength scanning PA measurements have less than 2% errors for the DQOCI dye [Fig. 2(a)] sample. The high-energy wavelength scanning mode serves as a basis for comparison of absorption spectra obtained with low-energy wavelength scanning and spectrally encoded PA measurements. In low-energy wavelength scanning mode, the laser pulse energy was reduced to ~3 nJ at 586 nm to mimic the achievable spectral density of a broadband photonics crystal supercontinuum fiber laser.[7] The low-energy wavelength scanning mode yielded a PA SNR of 3:1 at 586 nm. When the transient PA peak signal was mingled with the excessive noise, the amplitude of the Hilbert-transformed PA A-line signal did not accurately reflect the optical energy deposition distribution, yielding errors greater than 30%.

Using an S-sequence encoding mask [1 0 1 0 1 0 1 0 1 0 1 0 1 0 1] for
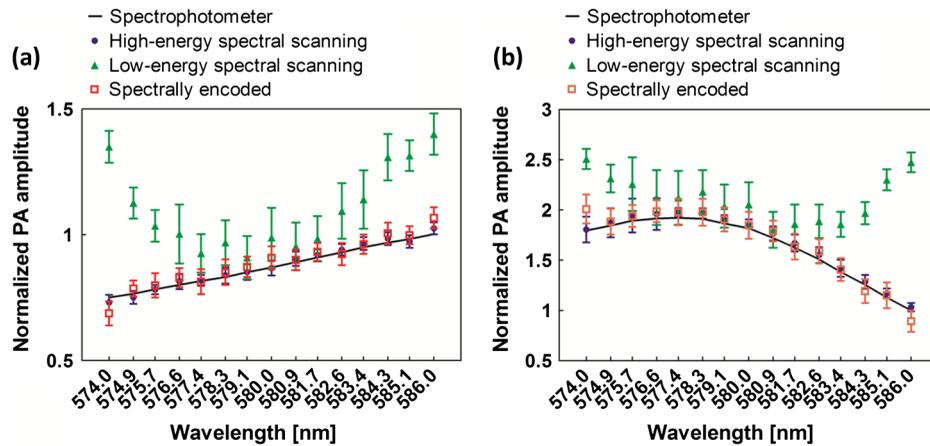
Fig. 2 Absorption spectra of (a) DQOCI dye and (b) bovine blood measured by a spectrophotometer and the photoacoustic imaging system in high-energy wavelength scanning, low-energy wavelength scanning, and spectrally encoded modes.

the spectrally encoded PA measurements, we selected eight wavelengths of 574.0, 575.7, 577.4, 579.1, 580.9, 582.6, 584.3, and 586.0 nm while maintaining the spectral density of the broadband dye laser beam the same as in the low-energy wavelength scanning mode. The PA A-line signal generated by the spectrally encoded PA measurements had a PA amplitude SNR of 38:1. In Fig. 2(a), the optical absorption coefficients of the DQOCI dye phantom measured by low-energy wavelength scanning are compared with those recovered by spectrally encoded PA measurements. The spectrally encoded PA measurements recovered the absorption coefficients over the range of wavelengths from 574 to 586 nm with less than 5% error. However, the low-energy wavelength scanning PA measurement showed 11% error from 577 to 583 nm. Below 577 nm and above 583 nm, where the laser pulse energy was relatively low, the error increased to >30%, which is explained by the low SNR of the PA A-line signals.

The experiment was repeated on a bovine blood sample. Figure 2(b) shows that the absorption spectrum reconstructed by the spectrally encoded PA measurement agreed with the spectrometer data with less than 6% error. The high-energy spectral scanning data had less than 3% error. But the low-energy spectral scanning data had 13% errors in the spectral range from 577 to 583 nm.

Further, blood vessels in a mouse ear were imaged *in vivo* as presented in Fig. 3. Unlike traditional optical spectroscopy and microscopy, PA microscopy acquires a time-of-flight signal, which provides depth profiling[16,17] for three-dimensional image formation by measuring the peak amplitudes of the Hilbert-transformed PA signals. Figure 3(a) shows the PA image stack consisting of images acquired in wavelength scanning modes. For the high-energy wavelength scanning measurement at 586 nm (an isosbestic point of oxyhemoglobin and deoxyhemoglobin), the PA amplitude SNR is 16:1 with a pulse energy of ~15 nJ. The pulse energy reduction to ~3 nJ at 586 nm decreased the PA amplitude SNR to 3:1 in low-energy wavelength scanning imaging. Figure 3(b) shows the DMD-encoding masks used in spectrally encoded PA measurements and the corresponding illumination spectra. By delivering eight wavelengths simultaneously, the spectrally encoded imaging mapped the blood vasculature with a PA A-line SNR of 36:1. Figure 3(c) and 3(d) shows the blood absorption spectra measured in the thin vessel (artery) and the thick vessel (vein),

respectively. The low-energy wavelength scanning PA measurements were inaccurate; the absorption spectrum represented no spectral features associated with hemoglobin absorption. In comparison, the spectrally encoded PA measurements allowed accurate reconstruction of the blood absorption spectra in the artery and vein, agreeing with the high-energy wavelength scanning PA measurements. From the spectrally encoded PA measurements of blood absorption, the map of blood oxygen saturation was recovered as shown in Fig. 3(e).[3] Both the high-energy wavelength scanning and the spectral encoding differentiated the artery and vein by quantifying the oxygen saturation of hemoglobin (SO$_2$). But the high-energy wavelength scanning failed due to its poor SNR. The superior performance of the spectrally encoded PA measurements is again attributed to the higher SNR of the PA amplitude when light beams of eight wavelengths were multiplexed.

By delivering eight wavelengths simultaneously, the SNR of the spectrally encoded PA structural image is improved approximately eight times. However, the spectrally encoded PA signal does not directly measure the absorption at individual wavelengths, because it includes illumination of eight wavelengths. In the matrix inversion operation to recover absorption spectra [Eq. (1)], noise propagation reduces the actual SNR gain in individual spectral elements to $(n + 1)/(2\sqrt{n})$ according to the multiplexing theory of Hadamard transformation optics.[13] For a mask containing $n = 15$ elements based on the S matrix, the SNR is increased by a factor of $(n + 1)/(2\sqrt{n}) = 2.1$ in comparison to filtering for one wavelength at a time. With DMD encoding, the spectral measurement accuracy for the DODCI solution and whole bovine blood samples was improved by ~2.2 times in the spectral range from 577 to 583 nm. Below 577 nm and above 583 nm, the improvement increased further. This further improvement may be attributed to the fact that the peak amplitude of the Hilbert-transformed PA A-line signal had too much contribution from noise when the SNR was low. The experimental results suggest that adequate SNRs of the spectrally encoded PA A-line signals allow more reliable spectral measurements. When n is further increased to include a broader spectral range, the SNR benefits of spectral encoding would become even greater.

In summary, we demonstrated a spectrally encoded PA microscopy system based on a DMD, which multiplexes wavelengths of illumination from a laser pumped circulating dye cell.
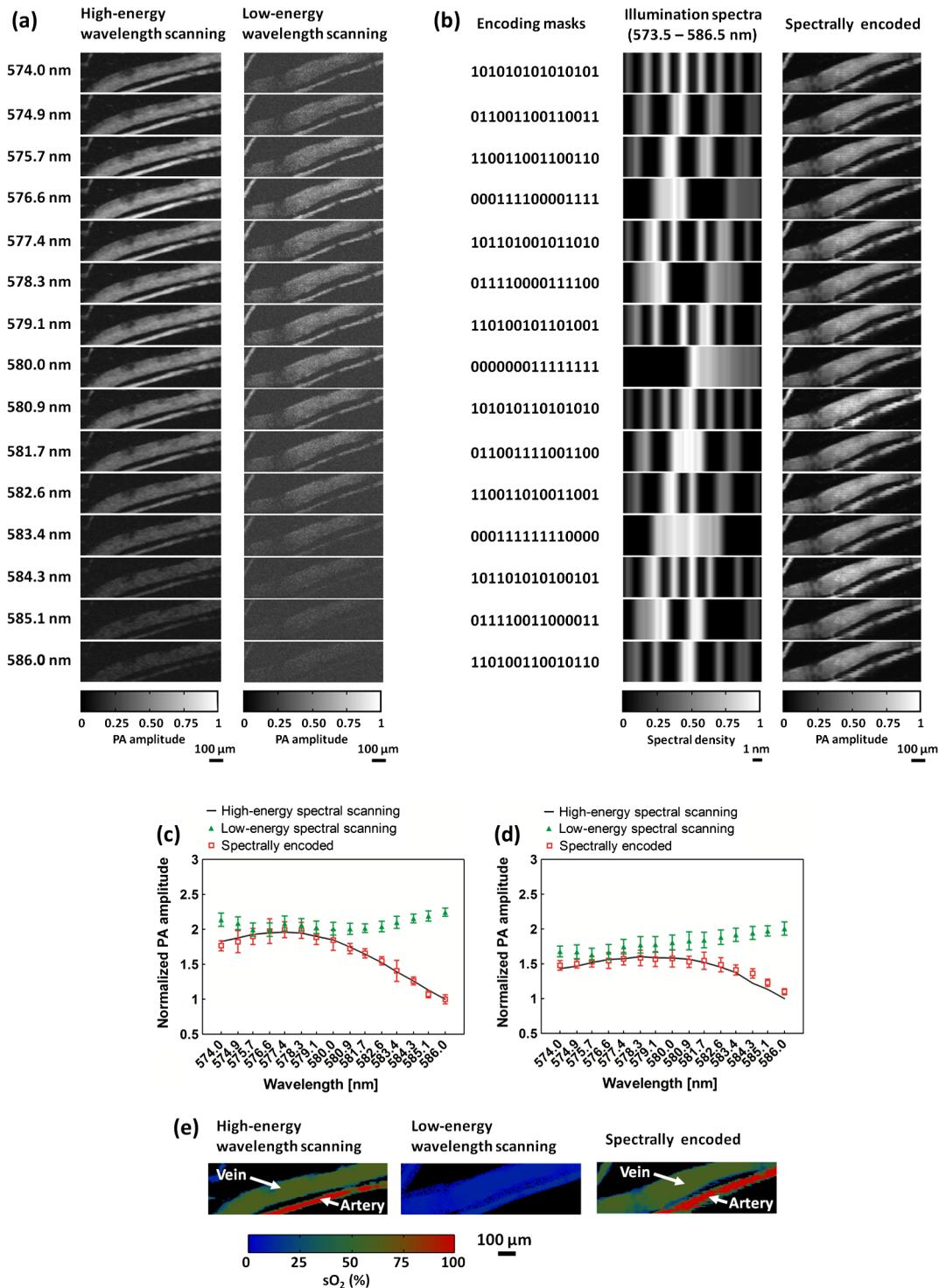
Fig. 3 (a) PA image stack of the blood vessels in a mouse ear acquired by high-energy wavelength scanning, low-energy wavelength scanning, and spectrally encoded PA microscopy. (b) DMD-encoding masks, corresponding illumination spectra and PA image stack of the blood vessels in a mouse ear acquired by spectrally encoded PA microscopy. (c) Blood absorption spectra in the thin vessel (artery). (d) Blood absorption spectra in the thin vessel (vein). (e) Comparison of SO₂ images acquired by high-energy wavelength scanning, low-energy wavelength scanning, and spectrally encoded PA microscopy.

The computer controllability of the DMD allows selection of multiple optical wavelengths at the laser pulse repetition rate up to 22 kHz, reducing the time to acquire a stack of multiwavelength PA images. Thus the spectrally encoded PA imaging system has the potential to spectrally image dynamic processes.

One example is blood oxygen release at the capillary level, imaged using hemoglobin absorption contrast.[3] A Hadamard encoding matrix multiplexed wavelengths in each broadband laser pulse. The optical absorption spectra were reconstructed by a complete set of PA measurements. Compared with the

wavelength-scanning method with the same number of measurements, the spectral-encoding method provides greater SNR by delivering multiple wavelengths simultaneously. Due to the multiplexing advantage, it is possible to use a broadband light source with decreased illumination power relative to that required for wavelength scanning. The results show that compact and relatively inexpensive light sources, such as a laser pumped dye cell, a photonic crystal fiber laser,[7] or a laser diode array,[9] combined with spectrally encoded PA measurements strategy, can be advantageously used for spectral PA imaging to resolve multiple types of absorbers.

Future work will explore supercontinuum light sources.[7,18] With a much broader visible and NIR wavelength spectrum, spectral encoding will give a significant SNR advantage over wavelength scanning. It is considered that this work represents the first step in improving multi-wavelength PA imaging speed by using broadband laser excitation systems.

Acknowledgments

References

1. D. Razansky et al., "Multispectral opto-acoustic tomography of deep-seated fluorescent proteins in vivo," *Nat. Photon.* **3**, 412–417 (2009).
2. L. V. Wang, "Multiscale photoacoustic microscopy and computed tomography," *Nat. Photon.* **3**, 503–509 (2009).
3. Y. Wang et al., "In vivo three-dimensional photoacoustic imaging based on a clinical matrix array ultrasound probe," *J. Biomed. Opt.* **17**, 061208 (2012).
4. K. H. Song et al., "Noninvasive in vivo spectroscopic nanorod-contrast photoacoustic mapping of sentinel lymph nodes," *Eur. J. Radiol.* **70**, 227–231 (2009).
5. R. Ma et al., "Multispectral optoacoustic tomography (MSOT) scanner for whole-body small animal imaging," *Opt. Express* **17**(24), 21414–21426 (2009).
6. H. R. Morris, C. C. Hoyt, and P. J. Treado, "Imaging spectrometers for fluorescence and raman microscopy: acousto-optic and liquid crystal tunable filters," *Appl. Spectrosc.* **48**(7), 857–866 (1994).
7. Y. N. Billeh, M. Liu, and T. Buma, "Spectroscopic photoacoustic microscopy using a photonic crystal fiber supercontinuum source," *Opt. Express* **18**(18), 18519–18524 (2010).
8. K. Maslov et al., "Optical-resolution photoacoustic microscopy for in vivo imaging of single capillaries," *Opt. Lett.* **33**(9), 929–931 (2008).
9. T. J. Allen and P. C. Beard, "Dual wavelength laser diode excitation source for 2D photoacoustic imaging," *Proc. SPIE* **6437**, 64371U (2007).
10. S. Sinha et al., "Spectral characteristics of a binary dye-mixture laser," *Appl. Opt.* **41**(33), 7006–7011 (2002).
11. J. P. Rice et al., "A hyperspectral image projector for hyperspectral imagers," *Proc. SPIE*, **6565**, 65650C (2007).
12. Y. Wang et al., "In vivo integrated photoacoustic and confocal microscopy of hemoglobin oxygen saturation and oxygen partial pressure," *Opt. Lett.* **36**(7), 1029–1031 (2011).
13. M. Harwit, "Hadamard transform techniques in spectroscopy and imaging spectroscopy," *Infrared Phys.* **17**(6), 457 (1977).
14. D. Xiang and M. A. Arnold, "Solid-state digital micro-mirror array spectrometer for Hadamard transform measurements of glucose and lactate in aqueous solutions," *Appl. Spectrosc.* **65**(10), 1170–1180 (2011).
15. G. Ku et al., "Photoacoustic microscopy with 2-microm transverse resolution," *J. Biomed. Opt.* **15**(2), 021302 (2010).
16. S. L. Wright, R. M. Hammaker, and W. G. Fateley, "Hadamard-transform photoacoustic spectrometry and depth profiling," *Appl. Spectrosc.* **47**, 272–276 (1993).
17. M. Sivaramakrishnan et al., "Limitations of quantitative photoacoustic measurements of blood oxygenation in small vessels," *Phys. Med. Biol.* **52**(5), 1349–1361 (2007).
18. D. Wildanger et al., "STED microscopy with a supercontinuum laser source," *Opt. Express* **16**(13), 9614–9621 (2008).